Desalination and Water Treatment
www.deswater.com
doi: 10.5004/dwt.2020.25173

182 (2020) 175–186
April

Hydrothermal synthesis of zeolite A and Y membrane layers on clay flat disc support and their potential use in the decontamination of water polluted with toxic heavy metals

Adnane Lahnafi[a], Abdelaziz Elgamouz[b,*], Najib Tijani[a], Ihsan Shehadi

[a]*Group Membranes, Matériaux et Procédés de Séparation, Faculté des Sciences, Université Moulay Ismaîl, Meknès, Morocco, email: aelgamouz@sharjah.ac.ae (A. Elgamouz)*
[b]*Department of Chemistry, College of Sciences, P.O. Box: 27272, Sharjah, University of Sharjah, United Arab Emirates*

Received 16 July 2019; Accepted 13 November 2019

ABSTRACT

The current paper presents the fabrication of new composite ceramic porous membranes by hydrothermal deposition of zeolite A (type LTA) (m-LTA) and Y (type Faujasite) (m-FAU) on clay support. Flat-disc membrane supports were prepared by uniaxial pressure on a mixture of clay and activated carbon (3.0%, w/w). The specific surface area of Faujasite-Y deposited was found to be 558.75 $m^2 g^{-1}$ with an average pore diameter of 20.90 Å, while zeolite-A was presented only with a specific surface area of 6.32 $m^2 g^{-1}$ and an average pore diameter of 128.70 Å. The structures of pores for both zeolite layers deposited were type IV according to IUPAC which are attributed to mesoporous solids. Scanning electron microscopy revealed that the edges of the cubes vary between 1.18 and 4.37 μm for the zeolite A (m-LTA) and the average diameter ranged between 0.98 and 3.03 μm for the zeolite Y (m-FAU). m-FAU membranes were found to perform better than m-LTA membranes. The rejection order for both membranes was $PbCl_2 > CoCl_2 > CdCl_2 > ZnCl_2$. For instance, a maximum rejection of 93% of $ZnCl_2$ was attained on m-FAU membranes in 1 h and 30 min membrane operation. However, the same rejection rate for the same metal salt was attained on m-LTA after 3 h and 30 min. The mechanism of metal salt rejection was dominated by the hydrated ionic size of cations, with an exception for $CoCl_2$ where rejection could be governed by repulsion between the charged ion and the membrane charged surface.

Keywords: Zeolite; Clay minerals; Ion size; Membranes; Heavy metals; Charge repulsion

1. Introduction

The removal of heavy metals from wastewaters is a major anxiety because of the high toxicity they can cause to the environment [1]. Damaging results could be obtained when toxic metals are available at contaminated levels affecting, survival, reproduction and sometimes their behavior [2]. Decontamination of industrial effluents from toxic heavy metals is usually carried out through filtration by ceramic membranes mainly because of their strength, thermal stability and ability to work in aggressive media, such as acid-base strong solvents [2–6]. Ceramic membranes surpass antagonist polymeric membranes [8–10] and other physicochemical techniques such as physical and chemical adsorptions, bacterial biomass, electrodialysis, sedimentation, flocculation, and photocatalysis [7–12]. Various ceramic membranes have been fabricated from different materials including, alumina oxides, silicon carbides, zirconia, titania, as well as glassy materials [11–14]. Membranes could be used for the filtration of liquids as well as gasses [15–17]. In recent years tubular and planar ceramic membranes were used because of their additional performing parameters such as flux and

* Corresponding author.

efficiency, different layers were deposited on membrane supports to obtain asymmetrical membranes that present desirable mechanical strength and thermal shock resistance [13]. The main factors to consider when using membranes in water filtration are porosity, pore size, pore distribution, surface charge and degree of hydrophobicity [14,15]. Zeolite is porous materials that were used as adsorption media in membranes technology, they are deposited inside the pores of ceramic supports, in tubular or plane form [16]. An example of these membranes is the nucleation and growth of zeolite microcrystals on alumina supports. Pores and surface properties of the alumina support were found to affect the final properties of the zeolite-alumina composite membrane [17]. The arrangement of zeolite tetrahedra (TO_4; T = Si, Al) which share oxygen atoms lead to tunnels like structure enclosing cavities that could be occupied by water or metal ions during the filtration process. Zeolite can occur naturally and could be synthesized from different starting materials, the two main components are alumina and silica, the properties of the synthesized zeolites were highly dependent on the Si/Al ratio. For example, hydrophobic zeolites were obtained when a low Si/Al ratio was used in the synthesis and these were used for the removal of polar compounds [18]. While when a high ratio of Si/Al was used hydrophilic zeolite membranes were used [19–22]. The wide field of applications was unlocked based on these properties namely catalysis and composite membranes [16,22–24]. More than half of the commonly studied heavy metal cations are divalent cations, they are identified, as pollutants in the environment, and a comprehensive understanding of their removals using membranes is vital for the remediation [25].

We herein fabricated two composite membranes, clay-zeolite A (m-LTA) and clay-Faujasite (m-FAU) via a hydrothermal method on a plane shape-like membrane supports. The supports were fabricated from clay mixtures with 3% activated carbon which was used as a porogen agent. The two membranes were tested to selectively remove heavy metal divalent cations from feed solutions. To understand divalent cations mechanism removal on the membranes, we studied the removal of four cations; lead (Pb^{2+}), cobalt (Co^{2+}), cadmium (Cd^{2+}) and zinc (Zn^{2+}) chlorides as single solutions on the clay support alone and the two membranes m-LTA and m-FAU. By measuring the flux of three different granulometry of the clay supports and the rejection % of heavy metal cation, we verify the significant influence of the support on both the rejection of the divalent cations as well as the permeability of the membranes. Optimum conditions were formulated for such membrane fabrication.

Our prepared membranes perform better than ultrafiltration membranes, which demonstrated very poor metal rejection mainly due to their large pore size between 0.01 and 100 μm. In addition, our membranes were very permeable to $ZnCl_2$ and very selective to $PbCl_2$.

2. Experimental

2.1. Materials

Sodium hydroxide (NaOH, 99%), sodium chloride (NaCl, >99.5%), Hydrochloric acid (HCl, 37%), sodium silicate ($Na_2Si_3O_7$), aluminum hydroxide ($Al(OH)_3$), sodium aluminate ($NaAlO_2$), sodium orthosilicate (Na_4SiO_4), zinc chloride ($ZnCl_2$, 98%), lead chloride ($PbCl_2$, 98%), cobalt(II) chloride ($CoCl_2$, $6H_2O$, 98%), cadmium chloride ($CdCl_2$, 2.5 H_2O, >98%), were obtained from Somaprol chemicals and Laboratory Reagent Ltd., Casablanca, Morocco. All the chemicals were used as received without any further purification. Deionized water Millipore (resistance = 17.2 MΩ cm) was used throughout all experiments. polyethylene bottles were used throughout the mixing of the precursor solutions to avoid silicon addition from glassware.

2.2. Preparation of the clay membrane supports

Clay mineral was collected from the central region of Morocco, characterized previously [26], was made into small particles with three different granulometry; $\Phi \leq 63$ μm, $63 \leq \Phi \leq 160$ and $160 \leq \Phi \leq 250$ using AFNOR standardized sieves. 4.0 g of 3% (w/w) (activated carbon/clay) were introduced into a stainless-steel mold and pressed uniaxially under a pressure of 460 bars, flat discs like pellets with 40.0 mm in diameter and 2.0 mm thickness were obtained. The activated carbon and granulated clay were shacked thoroughly to assure homogeneity prior to pressing. The consolidation of the support was assured by the surface adsorbed and constitutional waters of the clay, therefore no water was added to the powders. The raw flat-disc membrane supports were calcined to a final temperature of 1,000°C, using an electric furnace (type NABER 2804) following a heating program developed based on physico-chemical phenomena occurring in the clay-based on thermal analysis (DTA, TGA and shrinkage analysis) [5,6].

2.3. Zeolite membranes preparation

The seeded liquid phase hydrothermal synthesis was used to prepare zeolite A and Y membranes on $160 \leq \Phi < 250$ granulometry activated carbon progenenated flat-disc support, based on their interesting porosity and pore characteristics [5]. Prior to synthesis, the clay support was polished from both sides with a 600 grit-sand paper to obtain smooth surfaces from both sides of the support, later it was washed with de-ionized water to remove dust created during the smoothing, then dried overnight in an oven at 100°C. The aluminosilicate precursor gel was poured into a Teflon lined stainless-steel autoclave, where the support flat-discs was immersed and kept in a horizontal position, the bottom face of the membrane was covered with a cling film so that zeolite deposition would be only on the top face. Then the autoclave was heated overnight to a temperature of 80°C. Two gels were prepared separately for zeolite A; the silicate precursor molar composition was (0.02 SiO_2, 0.14 NaOH, 2.00 H_2O) and alumina precursor molar composition was (0.02 $Al(OH)_3$, 0.20 NaOH, 4.00 H_2O). For zeolite Y, a germination gel composed of (0.0255 NaOH, 6.38×10^{-3} $NaAlO_2$, 0.28 H_2O and 0.02 Na_4SiO_4) and a growth gel composed of (8.75×10^{-4} NaOH, 0.04 $NaAlO_2$, 1.82 H_2O and 0.1252 Na_4SiO_4). The two precursors for each zeolite type were mixed in a beaker prior to adding them to the autoclave in the presence of the clay support and were heated to a final temperature of 80°C in an oven for a period of 24 h.

Membranes prepared on the clay-flat-disc were named (m-LTA) for zeolite A and (m-FAU) for zeolite Y. The as-

prepared zeolite membranes were dried in open air overnight, and then heated to a final temperature of 480°C. Heating was made between 22°C and 480°C at a heating rate of 5.0°C min^{-1} under atmospheric air. The cooling back to 22°C was made with a cooling rate of 5.0° min^{-1}. The purpose of this step is to consolidate the zeolite membrane [5].

2.4. Characterization Techniques of the clay-zeolite membranes

Adsorption of N_2 was used to characterize the pore structures of the composite membranes m-LTA and m-LTA. An ASAP2000 Micrometrics apparatus, (Merignac, France) was used to characterize the pore structures and the specific surface area of the supports as well as the membranes. Nitrogen adsorption isotherms were performed at pressures up to the bulk saturating vapor pressure P^0 and at a temperature of 77.35 K. The total pore volume, V_p ($cm^3\ g^{-1}$), were estimated as total intrusion volume at a pressure of about 0.31 bar. The specific surface S_{BET} ($m^2\ g^{-1}$) was obtained by the Brunauer–Emmet–Teller (BET) theory. The pores size distribution (PSD) curves were computed from the desorption branches of the isotherms using the Barrett–Joyner–Halenda (BJH) algorithm for pore diameters between 17 and 3,000 Å. The pores sizes, D (Å), were determined from the maxima of the PSD curves. The scanning electron microscopy (SEM) images were taken by a JEOL JSM 6400, (Tokyo, Japan) (operating at a voltage of 20 kV). Membranes were also characterized by X-ray diffraction (XRD) using a LabX Shimadzu XRD-6100 diffractometer with a copper anode and a graphite monochromator to select $CuK_{\alpha 1}$ radiation (λ = 1.540 Å). Data was recorded between 2θ = 2.5° to 40° in increasing steps of 0.03° and t = 1 s/step.

2.5. Water absorption and porosity

Total porosity permits assessments of the percentile of voids in the clay supports and composite membranes and provides information about the strength of the final product. Porosity in support flat disks and prepared m-LTA and m-FAU membranes was measured using Eq. (1), where m_d is dry sample mass and m_f is wet sample mass after dipping in water for 24 h.

$$P = \frac{m_f - m_d}{m_d} \times 100 \tag{1}$$

2.6. Measurement of the isoelectronic points of zeolite A and Y

0.2 g of the solid (zeolite A or Y) was suspended in 100 mL of 0.001 M NaCl and 1.0 mL of 0.3 M HCl. The suspension was stirred until pH stabilization was reached. Flow volumes of 50 µL of 0.3 M NaOH were added to the homogenized solution and the pH of the suspension was recorded after each addition and stabilization. Blank solutions were taken as supernatants of the two zeolites' suspensions and were titrated under the same conditions. The charge present on the surface of the zeolite (σ) was calculated from the titration curve of the zeolite and the blank using Eq. (2).

$$\sigma = \Delta V \times \frac{FC_B \times 10^{-4}}{A \times m_s}\left(\frac{\mu C}{cm^2}\right) \tag{2}$$

where F is Faraday constant (96,480 C mol^{-1}), A is the specific surface area of the zeolite material ($m^2\ g^{-1}$), C_B is the concentration of the base added (mol L^{-1}), m_s is the solid–liquid ratio of the zeolite in (g L^{-1}) and ΔV, is the volume variation.

2.7. Measurement of metal ions concentration from filtered solutions

A 7000 Series Shimadzu atomic absorption spectrophotometer was used with single element hollow-cathode-lamps for Pb, Co, Cd, and Zn. 10^{-4} mol L^{-1} stock solutions of metal-contaminated waters were prepared for single metals from chloride salts of all metal ions. Standard solutions were prepared by diluting a commercial solution (~1,000 ppm) of the appropriate metal ion. The flame was used in the detection and combustion was assured by acetylene and air.

2.8. Filtration tests

Filtration tests were performed in an assembly specifically designed for this purpose (Fig. 1). The filtration unit of the flat-disc zeolite membrane has three entrees a feed entry connected to the pump and controlled with a valve and a pressure gauge to regulate the flow rate of filtration, a retentate entry of the membrane attached to the stock tank and controlled also with a valve and a pressure gauge to maintain the bleed flow rate of the membrane equal to the filtrate flow rate. The permeate entry is opened to the air and permeate is collected in a beaker over a balance. A condenser spiral tube circulated the tank is used to circulate cold water and maintain the temperature constant. The experimental protocol and devices used to carry out the filtration measurements are shown in Fig. 1.

2.9. Calculation methods

Specific surface S_{BET} ($m^2\ g^{-1}$) was obtained by the BET theory. The PSD curves were computed from the desorption branches of the isotherms using the BJH algorithm for pore diameter between 17 and 3,000 Å. The rejection of heavy metal ions by the membrane was represented as a percent (%), the permeate concentration from metals and stock solution were determined by atomic absorption using calibration curves. The percentage of rejection was calculated from Eq. (3).

$$\%\ \text{Rejection} = \frac{C_{feed} - C_{permeate}}{C_{feed}} \times 100 \tag{3}$$

In Eq. (3), $C_{permeate}$ is the molar concentration of the permeate and C_{feed} is the concentration of the feed solution.

The filtrate flux rate (J) in $L \times m^{-2} \times h^{-1}$ was measured from Eq. (4).

$$J = \frac{V_{permeate}}{A_{filter} \times t} \tag{4}$$

In Eq. (4), $V_{permeate}$, is the volume of the metal ion solution filtrated through the membrane and A_{filter} is the area of filtration of the membrane calculated from Eq. (5).

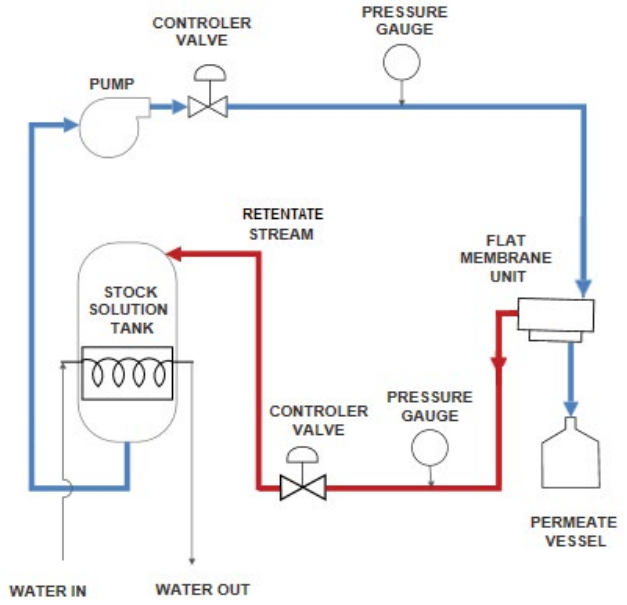

Fig. 1. Schematic representation for the filtration measurements.

$$A_{\text{filter}} = \pi \times \left(\frac{d}{2}\right)^2 = 7.07 \times 10^{-4}\,\text{m}^2 \quad (5)$$

In Eq. (5), d is the diameter of the filtration area which is equal to 3.0 cm.

3. Results and discussions

Analysis with XRD was carried out on the clay support alone prior to zeolite A and Y deposition. Figs. 2a and b show the raw and calcined clay material X-ray patterns. The predominantly clay mineral diffractions were identified by the inter-reticular measured distances, the Miller indices, and the 2θ position is given as follow: Quartz 4.27, (100), 20.9°; 3.35 (101), 26.7°; 2.45, (110), 36.5°, quartz diffractions were identified through powder diffraction File No 00-046-1045. Kaolinite 7.17, (00l), 12.3°; 4.47, (020), 19.8°; 3.57, (002), 24.8° and 2.38, (003), 37.9°, kaolinite diffractions were identified through powder diffraction file No 00-014-0164. Illite: 10.0, (002), 8.7°; 5.02, (004), 17.6° and 3.34°, (006), 26.6°, illite diffractions were identified through powder diffraction file No 00-026-0911. The presence of carbonate was noticed in

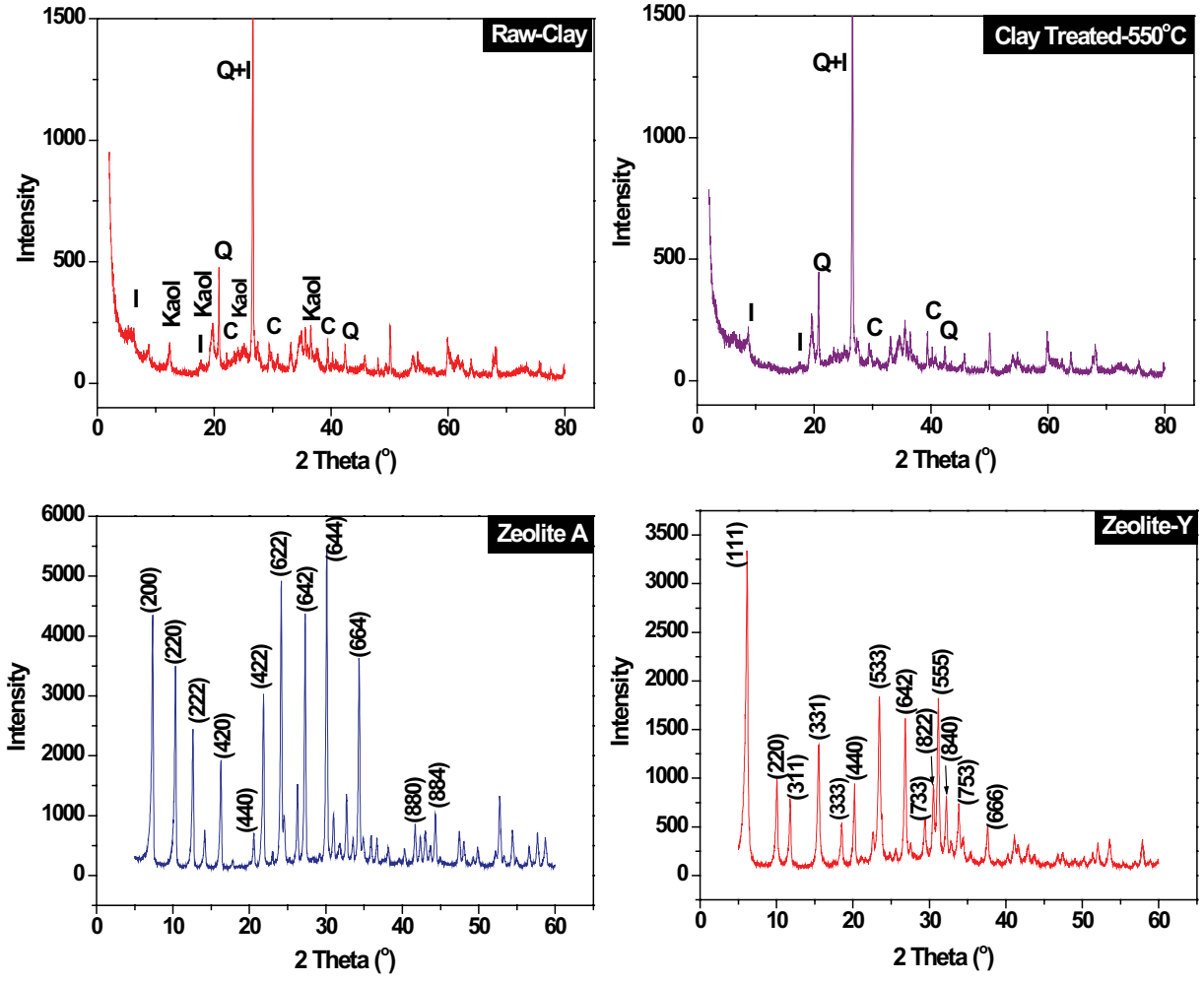

Fig. 2. X-ray diffractograms of raw clay material; treated and calcined clay material; zeolite A (Linde) and zeolite Y (type Faujasite).

the form of calcite and was identified by reflects of 3.84, (012), 23.1°; 3.04, (104), 29.4°; 2.83, (113), 39.5°. Calcite diffractions were identified through powder diffraction file No 00-005-0586.

Figs. 2c and d represent X-ray diffractograms of clay-zeolite A (m-LTA) and clay-Faujasite-Y (m-FAU) composite membranes. These patterns confirm essentially the formation of crystalline zeolite A and zeolite Y layers inside the pores as well as on the surface of the clay flat-disc supports without any preferred orientations. Diffraction pattern of zeolite A was consistent with zeolite A pattern type Linde (LTA) (powder diffraction File No 39-0222) [27] with peaks centered at 7.2°, 10.2°, 12.1°, 16.1°, 21.6°, 24.0°, 27.0°, 30.8°, 34.2° and 44.12° (2θ), which are indexed as the (200), (220), (222), (420), (442), (622), (642), (644), (664) and (884) reflections. While diffraction pattern of zeolite Y was consistent with those of zeolite type Y Faujasite (powder diffraction File No 00-043-0168), identified by eleven peaks centered at 6.2°, 10.4°, 11.2°, 18.7°, 20.3°, 23.6°, 26.9°, 29.6°, 30.7°, 31.3°, 32.4°, 33.0°, and 37.8° and indexed as (111), (220), (311), (331), (333), (440), (533), (642), (733), (822), (555), (840), (753) and (666) reflections.

SEM images were taken by a JEOL JSM 6400, (Tokyo, Japan) (operating at a voltage of 20 kV). Fig. 3 shows selected SEM micrograph images of the support made from 3% activated carbon as porogen and zeolite membranes synthesized on the support with typical Linde (LTA) morphology for zeolite A and Faujasite for zeolite Y. The presence of zeolite crystals were noticed inside the pores as well as on the surface of the 3% activated carbon porogenated clay flat-disc supports. Micrographs (a) and (b) represent the morphology of the 3% activated carbon porogenated flat-disc support showing that support has mixture of pores that could range from micro (<2.0 nm) to macro (>50.0 nm) size passing through meso ($2.0 < \Phi < 50.0$ nm). This was in accordance with a previous study where the size of the macropores was found to vary between 51.2 to 133 nm, while, the diameter of the mesopores was found to vary between 20.0 to 14 nm when the calcination temperature of a 3% activated carbon porogenated clay support was varying between 700°C to 950°C [5,6]. Micrographs (c) and (d) were obtained during the growth of zeolite A on the clay support. While (e) and (f) were obtained during the growth of zeolite Y on the same clay support. The morphology of zeolite A and Y are uniform and continuous throughout the surface of clay flat-discs. SEM pictures of zeolite A confirmed that crystals (Fig. 3d) were short cubes varying size between 1.18 to 4.37 μm in edge, while, zeolite Y crystals (Fig. 3f) were in the form of octahedral prisms with average diameter varying between 0.98 to 3.03 μm, some are aggregates with varying sizes. Similar results were obtained when imprinted zeolite-Y for p-cresol removal in hemodialysis were synthesized, the diameter was 0.38 μm while commercial zeolite Y was in the range of 0.45 μm [28].

The volume of nitrogen adsorbed at vapor pressure P^0 and temperature of 77.35 K for the clay support, m-LTA, and m-FAU membranes was measured using the ASAP2000 Micrometrics apparatus, plots of the hysteresis loops were plotted against the relative pressure (Fig. 4). The hysteresis loop for the clay support correspond to those of type H3 according to the IUPAC classification [29], this is an indication that the membrane supports are in large macroporous, with "slot" like pores; formed by the superposition of crystalline platelets which are originated from clay phyllosilicate structures [26,30]. While the hysteresis was of type H4 for both membranes m-LTA and m-FAU, which characterize mesoporous materials, a broad hysteresis was obtained in the case of m-FAU while m-LTA condensation branch was almost superimposed to the evaporation branch.

The structural parameters derived from the nitrogen adsorption isotherms are reported in Table 1. The specific surface area dropped from 71.2 $m^2\ g^{-1}$ for the clay powder used in the preparation of the clay support to 0.393 $m^2\ g^{-1}$ for the $160 \le \Phi < 250$ granulometry support. This dramatic decrease was mainly due to the compacting and the calcination of the support to 1,000°C. The volume of the pores followed the same trend as decreasing from 0.1151 to 0.00082 $cm^3\ g^{-1}$ for the clay powder and the $160 \le \Phi < 250$ granulometry support respectively. As far as the zeolite membranes were concerned, the deposition of zeolite on the clay support leads to an increase in the BET specific surface area (S_{BET}, $m^2\ g^{-1}$) from 0.393 $m^2\ g^{-1}$ for the clay support to 6.3 and 558.8 $m^2\ g^{-1}$ for m-LTA and m-FAU respectively, indicating that deposition of zeolite A and Y is responsible for this dramatic increase. The total pore volume (V_p, $cm^3\ g^{-1}$) also, was found to increase by deposition of zeolite material on clay support. The total pore volumes were found to increase from 0.00082 $cm^3\ g^{-1}$ for the clay support to 0.0240 and 0.1068 $cm^3\ g^{-1}$ for m-LTA and m-FAU membranes respectively. The average pore diameters (D_p, Å) however, were found to decrease by depositing zeolite Y inside the pores of the clay supports. The average pore diameter decreased from 74.4 Å for the support to 20.9 Å for m-FAU; however, the increase in the pore diameter was assessed in the case of m-LTA. An increase in the specific surface area ought to be faced with an increase in the pores' volume, as the specific surface included the external surface of the material (exposed) as well as the surface of the pores' walls. However, this was not the case as it was demonstrated from a previous work that mesopores contribute to the specific surface area more than macropores [5,6]. The channels of the zeolite must have a direct effect on the pores' volume and dimeter; for instance, faujasite has a narrow pore channel compared to zeolite A which presents mesopores.

The water porosity of the support and membranes was measured and found to be 11.80 ± 0.24, 9.67 ± 0.19, 10.69 ± 0.21 for the clay support, m-LTA and m-FAU membranes respectively. The support was presented with high porosity followed by m-FAU then m-LTA, these values are directly linked to the capillary movement of water in the support and membranes pores that are opened to the outside. Porosity of the clay support was lower as compared to previously reported fired supports due to grains fusion at high temperatures leading to the reduction of macropores and mesopores grid which is responsible for holding water [31].

The isoelectronic points of both zeolite were determined from the curve of titration of zeolite A and Y represented in Fig. 5. The values of the isoelectronic points were $pHpzc_A = 11.3$ and $pHpzc_Y = 11.4$ for zeolite A and Y suspensions respectively. In general, surface charges for both suspensions given in Fig. 5, were found to drop down with increasing the pH, similar behavior was found by Lui

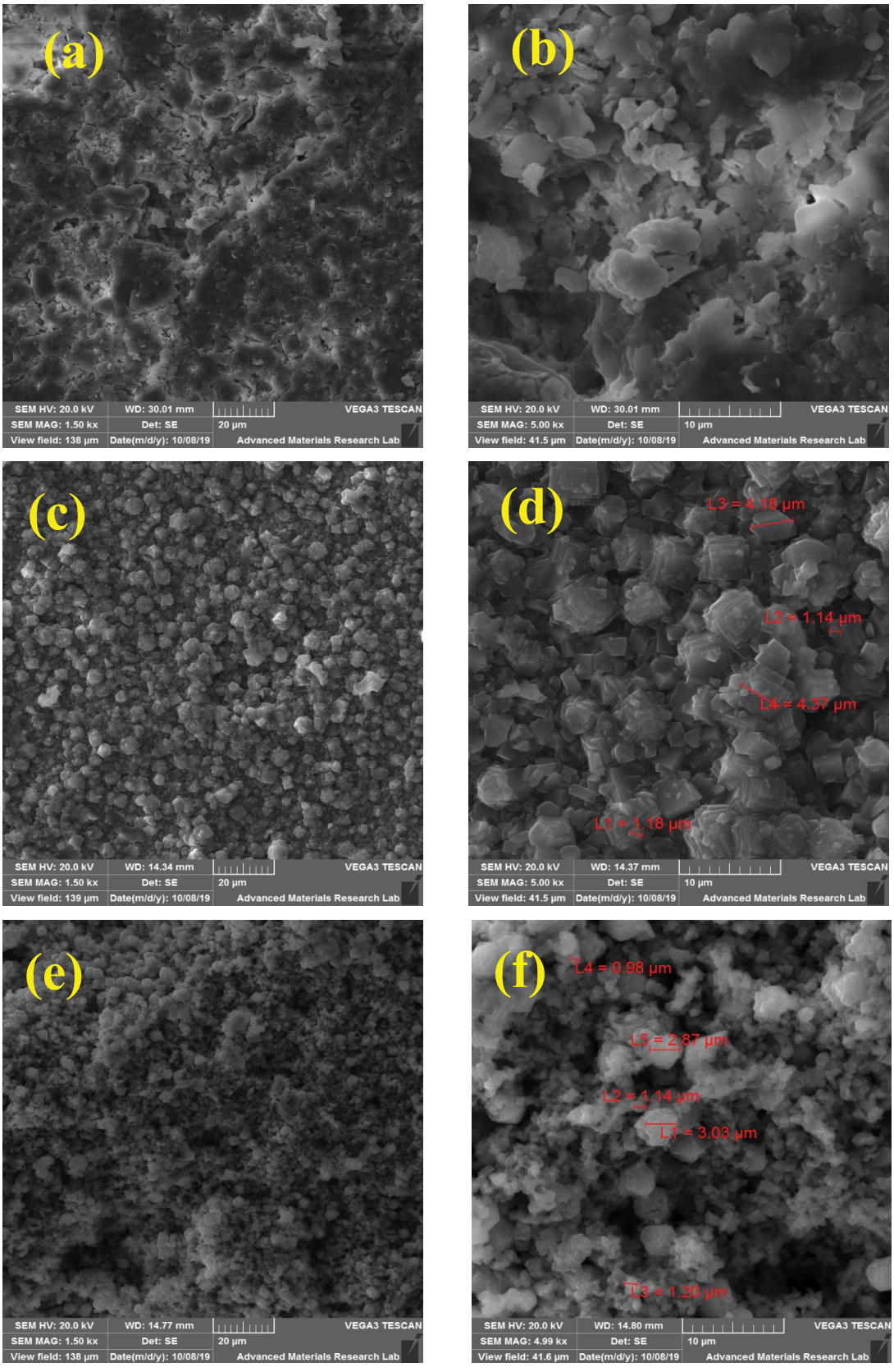

Fig. 3. SEM micrographs of (a) x1.50 K magnification and (b) 5.00 K magnification of the porogenated activated carbon clay support; (c) and (d) micrographs of m-LTA at x1.50 K and 5.00 K magnification respectively; (e) and (f) micrographs of m-FAU at x1.5 K and x5.00 K magnification respectively.

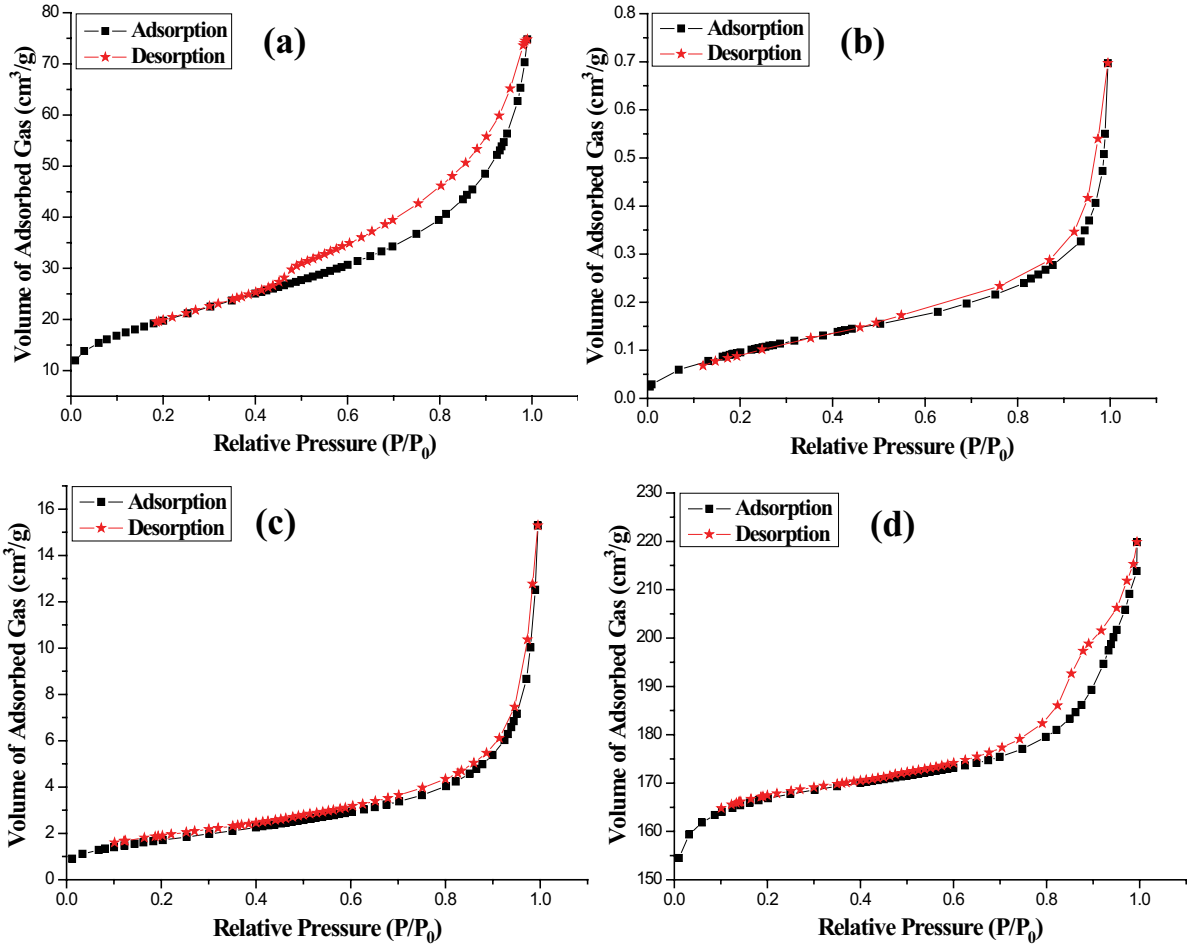

Fig. 4. Nitrogen sorption of (a) clay powder used for the fabrication of the clay supports, (b) membrane supports made from 160 ≤ Φ < 250 granulometry clay and 3% activated carbon, (c) m-LTA membrane, and (d) m-FAU membrane.

Table 1
Structural parameters derived from the isotherms of N_2 adsorption of clay support, m-LTA and m-FAU membranes

	S_{BET} ($m^2\ g^{-1}$)	V_p ($cm^3\ g^{-1}$)	D_t (Å)
Clay Powder	71.2	0.1151	69.6
160 ≤ Φ ≤ 250 support	0.393	0.00082	74.4
m-LTA	6.3	0.0240	128.7
m-FAU	558.8	0.1068	20.9

et al. [32] when studying zeta potential of beta zeolites as a function of the pH.

Prior to the filtration of metal ions through the two zeolite membranes m-LTA and m-FAU, the flat disc supports were mounted in the pilot and flux experiments were conducted as a function of time using de-ionized water. Fig. 6a represents the evolution of flux as a function of time for three membrane clay supports with three different granulometry; Φ < 63 μm, 63 ≤ Φ < 160 and 160 ≤ Φ < 250.

The supports experienced a significant water flux increase with increasing the granulometry of the clay material used in the fabrication of the supports, initial flux of 430.4 ± 8.61, 636.5 ± 12.73and 1,039 ± 20.78 L $m^{-2}\ h^{-1}$ were obtained for Φ < 63 μm, 63 ≤ Φ < 160 and 160 ≤ Φ < 250 granulometries respectively with 41% increase from Φ < 63 granulometry to 160 ≤ Φ < 250 granulometry. This increase is attributed to the expansion of the nanochannels that allow more water molecules to flow through the membrane support at a faster rate. The flux decreases after 4 h of operation by 25.1%, 37.0% and 40.0% for the three granulometries respectively. The result indicates that with high granulometry more permeation pathways are formed in the membrane support. Hence the 160 ≤ Φ < 250 granulometry was used for the deposition of zeolite A and zeolite Y. The deposition of zeolite on the support leads to narrowing the pore channels in both membranes m-LTA and m-FAU. Such an argument is demonstrated in Fig. 6b which shows a decrease in the initial flux from 1,039 ± 20.78 L $m^{-2}\ h^{-1}$ for 160 ≤ Φ < 250 granulometry clay support to 462.90 ± 9.26 and 628.63 ± 12.57 for both membranes m-LTA and m-FAU respectively. The final flux was decreased by 60.00%, 79.90%, and 68.12% respectively for the clay support, m-LTA and m-FAU, hence showing that fouling follows the trend m-LTA > m-FAU > clay support. The m-LTA was presented with the highest fouling compared to m-FAU even though m-LTA pore diameter (128.7 Å) was 6 times larger than m-FAU average diameter of 20.9 Å.

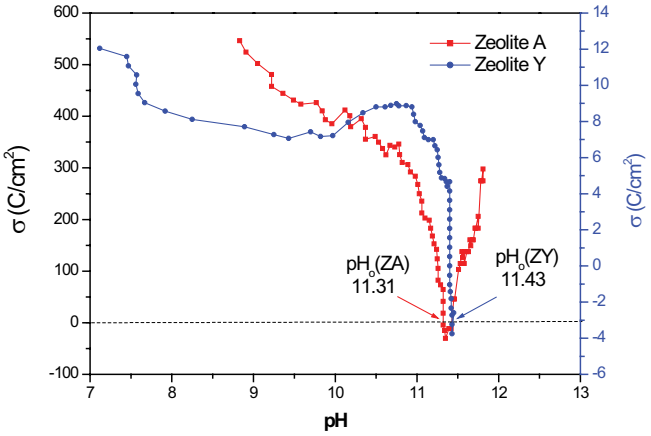

Fig. 5. Surface charge curves of zeolite A and Y suspensions at ionic strength 0.001 M.

This could be attributed to the fact that faujasite has narrow pore channels compared to the mesopores zeolite A. The separation performance of the 160 ≤ Φ < 250 granulometry clay support and m-LTA and m-FAU composite membranes for typical heavy metal chloride salts aqueous solutions was investigated separately with a concentration of 10^{-4} mol L^{-1} and under pressure of 0.5 bar. Figs. 7a–c show the flux of support, m-LTA and m-FAU membranes of the four heavy metals salts solutions. The heavy metals solutions initial flux were found to drop by 6.97%, 16.48%, 24.26%, and 30.67%; 45.90%, 60.71%, 74.18%, 80.05% and 19.43%, 33.55%, 51.90%, 57.69% for Pb^{2+}, Co^{2+}, Cd^{2+} and Zn^{2+} when compared with initial water flux on the clay support, m-LTA and m-FAU respectively. Showing that m-LTA was presented by the highest fouling of heavy metals. Percent of rejection of the support and the two membranes m-LTA and m-FAU are presented in Figs. 7d–f, the rejection of different salts were found to be in the order of $PbCl_2$ > $CoCl_2$ > $CdCl_2$ > $ZnCl_2$, their corresponding values after 3.5 h operation were (99.22%, 97.91%, 79.83% and 71.56%); (98.96%, 97.92%, 93.95% and 92.68%) and (99.30%, 98.93%, 95.15% and 94.08%) for clay support, m-LTA and m-FAU respectively. Rejection of Pb^{2+} and Co^{2+} was almost similar for the clay supports and the two zeolite membranes with rejection percentages of more than 98%. However, rejection of Cd^{2+} and Zn^{2+} on the support was lower than rejection on zeolite membranes with the highest rejection presented by m-FAU for both metals. Rejection of metal cations is dominated by the hydrated ionic size of cations, except cobalt. The metal-oxygen distance (M–O) in Å and configuration of hydrated metal cations used are (2.54, $Pb(H_2O)_6^{2+}$)); (2.08, $Co(H_2O)_6^{2+}$ and 1.87 for $Co(H_2O)_6^{3+}$); (2.3, $Cd(H_2O)_6^{2+}$); (2.08, $Zn(H_2O)_6^{2+}$) [33]. The cobalt exception could find an explanation in the fact that the membrane charge played an important role among other factors in the rejection behavior of the clay support. At a particular pH of the feed solution, the membrane charge is greatly influenced [34]. The rejection of heavy metal cations on zeolite Y was found to be slightly higher than zeolite A. The rejection mechanism of both membranes (m-LTA and m-FAU) is beyond sieving which relies on the size of the hydrated metal ions, rejection could be governed by repulsion between the charged ion and the membrane charged surface [35]. This is true for both membranes as the metallic feed solutions are acidic (pH < $pHpzc_A$ = 11.31 and $pHpzc_Y$ = 11.41), and the two membranes would develop positive charges on their surfaces which repulse the divalent cations. Similar results were found by Gherasim and Mikulášek [36,37] when studying the removal of Pb^{2+} from aqueous solution on a commercial nanofiltration membrane (AFC 80). It was found that the charge on the surface of the membrane was pH dependent and Pb^{2+} rejection was partially dependent on mutual repulsion between the membrane and Pb^{2+}. Zeolites are known also, to have a higher cation exchange capacity (CEC), hence they are widely used as a cation exchanger. The order of rejection of both zeolites was found to follow the same behavior of zeolite exchanger (Pb^{2+} > Cd^{2+} > Zn^{2+}), this order

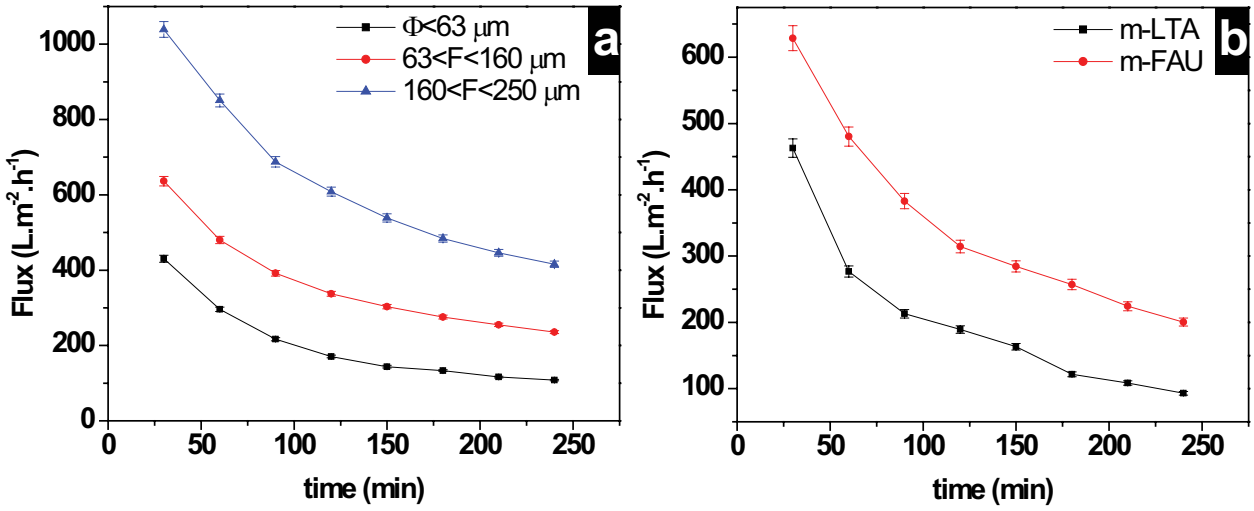

Fig. 6. (a) Water flux measurement of the 3% porogenated activated carbon clay supports made from different granulometry; Φ < 63 μm, 63 ≤ Φ < 160 and 160 ≤ Φ < 250 and 160 ≤ Φ < 250 fired to 1,000°C and (b) water flux measurement of the two membranes m-LTA and m-FAU, water flow rate (F_w = 1.00 × 10^{-2} L h^{-1}), filtration surface (A = 7.07 × 10^{-4} m^2) and pressure P = 0.5 bar.

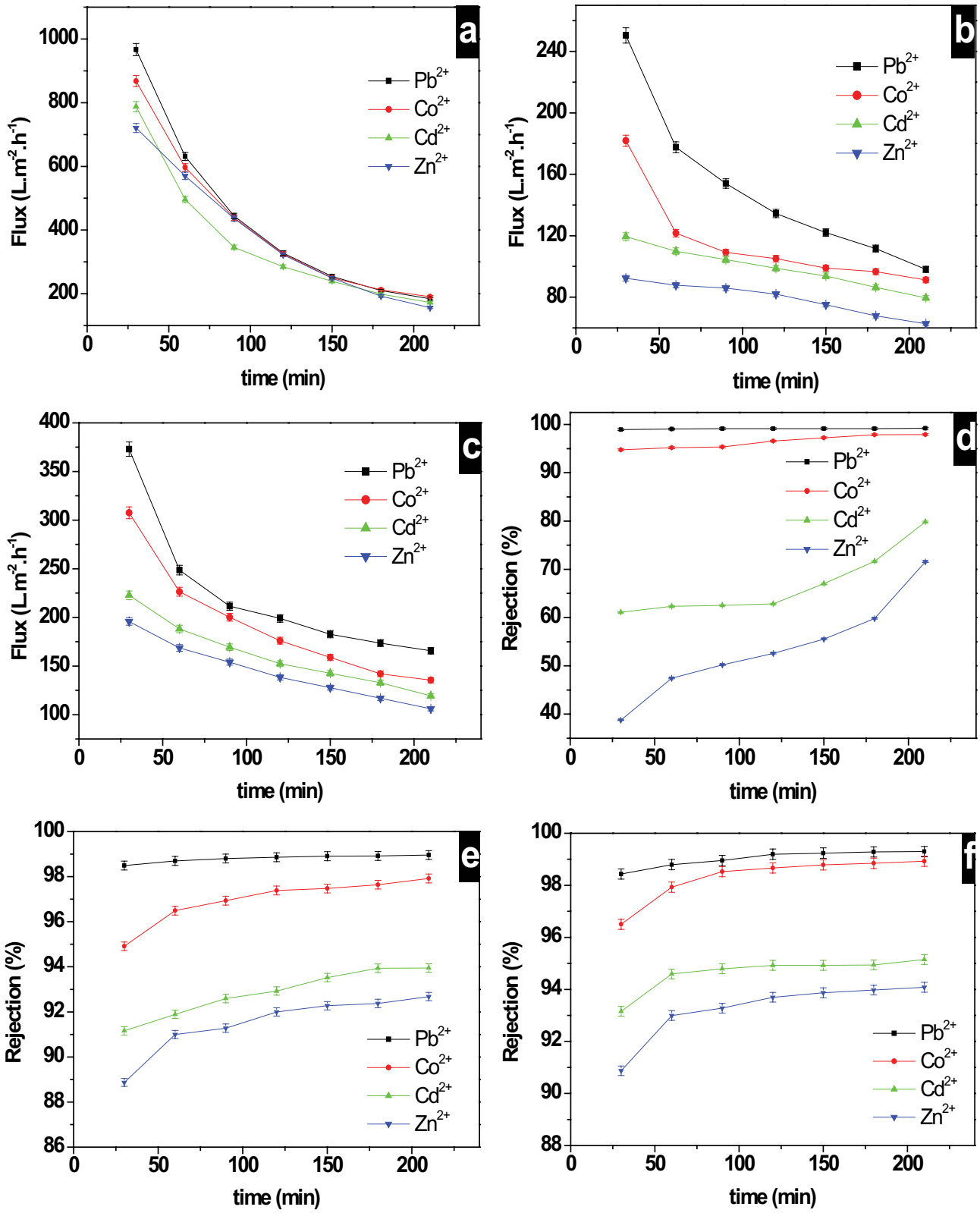

Fig. 7. Flux measurement and retention of (a,d) 3% porogenated activated carbon clay support made from 160 ≤ Φ < 250 granulometry; (b,e) m-LTA membrane; (c,f) m-FAU membrane, water flow rate (F_w = 1.00 × 10^{-2} L h^{-1}), filtration surface (A = 7.07 × 10^{-4} m^2) and pressure P = 0.5 bar.

Table 2
Removal of heavy metals by nanofiltration membranes compared to m-LTA and m-FAU fabricated membranes

Heavy metal	Membrane	pH	Concentration of heavy metal (mg L^{-1})	Rejection (%)	References
Pb^{2+}	AFC80	5.7	50.0	99.4	[40]
Cu^{2+}				47.9	
Cd^{2+}	PVDF/APTES	5.5	5.0	44.2	[41]
Cr^{6+}				52.3	
Pb^{2+}	PSf	5.8	250	98.0	[36]
Ni^{2+} Cr^{6+}	PAN/TiO_2	NA	50	88.1	[42]
Pb^{2+}		4.8		99.5	
Cd^{2+}		4.7		98.3	
				99.7	
Ni^{2+}	P84	5.8	1,000	93.5	[43]
Cr^{3+}		4.9		99.5	
As^{5+}		7.7			
Pb^{2+}		7.2	20.7	99.0	
Co^{2+}		7.6	5.9	97.9	
Cd^{2+}	m-LTA	7.1	11.4	94.0	This work
Zn^{2+}		7.6	6.5	93.0	
Pb^{2+}		7.2	20.7	99.3	
Co^{2+}		7.6	5.9	98.9	
Cd^{2+}	m-FAU	7.1	11.4	95.2	This work
Zn^{2+}		7.6	6.5	94.1	

was explained based on the Si/Al ratio in the zeolite, high Sil/Al ratio results in low anionic field which give rise to high selectivity for cations with lower charges [38]. Also, to size exclusion and mutual repulsion removal mechanisms, cations may have been adsorbed by the membrane surface. Bouranene et al [39] found while studying the rejection of cobalt and lead on a polyamide nanofiltration membrane, that the divalent cation was not only found to be adsorbed on the surface of the membrane but also modifying its charge.

The percent rejections of the divalent cations studied on both membranes were comparable to heavy metal cations rejection by various nanofiltration membranes reported in Table 2. However, our prepared membranes perform better than ultrafiltration membranes, which demonstrated very poor metal rejection mainly due to their large pore size between 0.01 and 100 μm. [14].

4. Conclusion

Preparation of clay zeolite composite membranes on 3% activated carbon porogenated support from a widely available clay material was successfully achieved with the hydrothermal methodology. The crystal phases of the zeolites A and Y were identified using XRD and SEM. The pores' structures of the supports and the composite membranes were characterized using nitrogen adsorption and BJH algorithm while specific surface area by using the BET method. Flux studies of the membrane support helped in choosing the convenient support for zeolite deposition. Pore size was directly influenced by the granulometry of the clay starting material used for the fabrication of the clay supports. Undeniably the $160 \leq \Phi < 250$ granulometry presented wide pores which were more convenient to zeolite deposition showing that more permeation pathways were formed in the membrane support. Rejections of more than 90% were obtained for all heavy metal pollutants filtered on both zeolite membranes. The membranes were very permeable to $ZnCl_2$ and very selective to $PbCl_2$. The mechanism by which the two membranes function was found to be dominated by the hydrated cation size however other mechanisms such as the charge repulsion between the cation and isoelectronic point of the membrane or the cationic exchange capacity of the zeolite could be used to explain the behavior of the membrane during the separation of $CoCl_2$.

Acknowledgment

This work was supported by "Centre National pour la Recherche Scientifique et Technique/Rabat, Morocco (CNRST) under grant category PPR2. The authors wish also to thank the Center of Advanced Materials Research - University of Sharjah for analysis.

References

[1] G. Hu, J. Cao, Metal-containing nanoparticles derived from concealed metal deposits: an important source of toxic

nanoparticles in aquatic environments, Chemosphere, 224 (2019) 726.
[2] M.C. Reiley, Science, policy, and trends of metals risk assessment at EPA: how understanding metals bioavailability has changed metals risk assessment at US EPA, Aquat. Toxicol., 84 (2007) 292.
[3] J. Kujawa, S. Cerneaux, W. Kujawski, Investigation of the stability of metal oxide powders and ceramic membranes grafted by perfluoroalkylsilanes, Colloids Surf., A, 443 (2014) 109.
[4] T. Wu, N. Wang, J. Li, L. Wang, W. Zhang, G. Zhang, S. Ji, Tubular thermal crosslinked-PEBA/ceramic membrane for aromatic/aliphatic pervaporation, J. Membr. Sci., 486 (2015) 1–9.
[5] A. Elgamouz, N. Tijani, From a naturally occurring material (clay mineral) to the production of porous ceramic membranes, Microporous Mesoporous Mater., 271 (2018) 52–58.
[6] A. Elgamouz, N. Tijani, Dataset in the production of composite clay-zeolite membranes made from naturally occurring clay minerals, Data Brief, 19 (2018) 2267.
[7] M. Huang, J. Pan, L. Zheng, Removal of heavy metals from aqueous solutions using bacteria, J. Shanghai Univ. (English Ed.), 5 (2001) 253.
[8] J. Koelmel, M. Prasad, G. Velvizhi, S.K. Butti, S.V. Mohan, In: M.N.V. Parasad Kaimin Shih, Ed., Metalliferous Waste in India and Knowledge Explosion in Metal Recovery Techniques and Processes for the Prevention of Pollution, Environmental Materials and Waste, Elsevier, London, 2016, pp. 339–390.
[9] H. Rabiee, K.R. Khalilpour, J.M. Betts, N. Tapper, in: K.R. Khalilpour, Ed., Energy Water Nexus: Renewable-Integrated Hybridized Desalination Systems, Polygeneration with Polystorage for Chemical and Energy Hubs, Elsevier, London, 2019, pp. 409–458.
[10] S. Kempton, R.M. Sterritt, J.N. Lester, Heavy metal removal in primary sedimentation I. The influence of metal solubility, Sci. Total Environ., 63 (1987) 231.
[11] T. Hou, H. Du, Z. Yang, Z. Tian, S. Shen, Y. Shi, W. Yang, L. Zhang, Flocculation of different types of combined contaminants of antibiotics and heavy metals by thermo-responsive flocculants with various architectures, Sep. Purif. Technol., 223 (2019) 123–132.
[12] Y. Xu, C. Zhang, P. Lu, X. Zhang, L. Zhang, J. Shi, Overcoming poisoning effects of heavy metal ions against photocatalysis for synergetic photo-hydrogen generation from wastewater, Nano Energy, 38 (2017) 494.
[13] A. Chougui, K. Zaiter, A. Belouatek, B. Asli, Heavy metals and color retention by a synthesized inorganic membrane, Arab. J. Chem., 7 (2014) 817.
[14] N. Abdullah, N. Yusof, W.J. Lau, J. Jaafar, A.F. Ismail, Recent trends of heavy metal removal from water/wastewater by membrane technologies, J. Ind. Eng. Chem., 76 (2019) 17.
[15] A. Jona, Characterization of pore structure of filter media, Fluid Part. Sep. J., 14 (2002) 227.
[16] J.S. Beck, J.C. Vartuli, W.J. Roth, M.E. Leonowicz, C.T. Kresge, K.D. Schmitt, C.T.-W. Chu, D.H. Olson, E.W. Sheppard, S.B. McCullen, J.B. Higgins, J.L. Schlenker, A new family of mesoporous molecular sieves prepared with liquid crystal templates, J. Am. Chem. Soc., 114 (1992) 10834.
[17] R.S. Dariani, M. Nazari, Comparison of stress, strain, and elastic properties for porous silicon layers supported by substrate and corresponding membranes, J. Mol. Struct., 1119 (2016) 308.
[18] C. Wang, S. Leng, H. Guo, L. Cao, J. Huang, Acid and alkali treatments for regulation of hydrophilicity/hydrophobicity of natural zeolite, Appl. Surf. Sci., 478 (2019) 319.
[19] S. Aguado, A.C. Polo, M.P. Bernal, J. Coronas, J. Santamaría, Removal of pollutants from indoor air using zeolite membranes, J. Membr. Sci., 240 (2004) 159.
[20] J. Coronas, J. Santamaria, Separations using zeolite membranes, Sep. Purif. Methods, 28 (1999) 127.
[21] J.D. Ramsay, Characterization of the pore structure of membranes, MRS Bull., 24 (1999) 36.
[22] M.P. Bernal, J. Coronas, M. Menéndez, J. Santamaría, Characterization of zeolite membranes by measurement of permeation fluxes in the presence of adsorbable species, Ind. Eng. Chem. Res., 41 (2002) 5071.
[23] M.A. Ulla, R. Mallada, J. Coronas, L. Gutierrez, E. Miró, J. Santamarıa, Synthesis and characterization of ZSM-5 coatings onto cordierite honeycomb supports, Appl. Catal., A, 253 (2003) 257.
[24] B.T. Holland, L. Abrams, A. Stein, Dual templating of macroporous silicates with zeolitic microporous frameworks, J. Am. Chem. Soc., 121 (1999) 4308.
[25] Z. Li, Z. Ma, van der Kuijp, T. Jan, Z. Yuan, L. Huang, A review of soil heavy metal pollution from mines in China: pollution and health risk assessment, Sci. Total Environ., 468 (2014) 843.
[26] A. El Gamouz, H. Bendifi, M. El Amane, L. Messaoudi, N. Tijani, Physico-chemical characterisation of a clay rock from MeknesTafilalet region, Phys. Chem. News, 34 (2007) 120.
[27] Y.P. de Peña, W. Rondón, Linde type a zeolite and type Y Faujasite as a solid-phase for lead, cadmium, nickel and cobalt preconcentration and determination using a flow injection system coupled to flame atomic absorption spectrometry, Am. J. Anal. Chem., 4 (2013) 387.
[28] Y. Raharjo, A.F. Ismail, M.H.D. Othman, Malek, N.A.N. Nik, D. Santoso, Preparation and characterization of imprinted zeolite-Y for p-cresol removal in haemodialysis, Mater. Sci. Eng., C, 103 (2019) 109722.
[29] M. Arruebo, J. Coronas, M. Menendez, J. Santamarıa, Separation of hydrocarbons from natural gas using silicalite membranes, Sep. Purif. Technol., 25 (2001) 275.
[30] E. Mateo, M. Menendez, J. Coronas, N. Tijani, H. Ahlafi, L. Messaoudi, A. El Gamouz, M. Ouammou, Preparation and characterization of moroccan clay support for zeolitic membranes, Phys. Chem. News, 44 (2008) 15.
[31] A. Elgamouz, N. Tijani, I. Shehadi, K. Hasan, M. Al-Farooq Kawam, Characterization of the firing behaviour of an illite-kaolinite clay mineral and its potential use as membrane support, Heliyon, 5 (2019) e02281.
[32] X. Liu, P. Mäki-Arvela, A. Aho, Z. Vajglova, V. Gun'ko, I. Heinmaa, N. Kumar, K. Eränen, T. Salmi, D.Y. Murzin, Zeta potential of beta zeolites: influence of structure, acidity, pH, temperature and concentration, Molecules, 23 (2018) 946.
[33] I. Persson, Hydrated metal ions in aqueous solution: how regular are their structures?, Pure Appl. Chem., 82 (2010) 1901.
[34] D. Qadir, H.B. Mukhtar, L.K. Keong, Rejection of divalent ions in commercial tubular membranes: effect of feed concentration and anion type, Sustainable Environ. Res., 27 (2017) 103.
[35] Z.V.P. Murthy, L.B. Chaudhari, Separation of binary heavy metals from aqueous solutions by nanofiltration and characterization of the membrane using Spiegler–Kedem model, Chem. Eng. J., 150 (2009) 181.
[36] C. Gherasim, P. Mikulášek, Influence of operating variables on the removal of heavy metal ions from aqueous solutions by nanofiltration, Desalination, 343 (2014) 67.
[37] C. Gherasim, J. Cuhorka, P. Mikulášek, Analysis of lead(II) retention from single salt and binary aqueous solutions by a polyamide nanofiltration membrane: experimental results and modelling, J. Membr. Sci., 436 (2013) 132.
[38] A. Langella, M. Pansini, P. Cappelletti, B. de Gennaro, M. de'Gennaro, C. Colella, NH_4^+, Cu^{2+}, Zn^{2+}, Cd^{2+} and Pb^{2+} exchange for Na^+ in a sedimentary clinoptilolite, North Sardinia, Italy, Microporous Mesoporous Mater., 37 (2000) 337.
[39] S. Bouranene, P. Fievet, A. Szymczyk, M. El-Hadi Samar, A. Vidonne, Influence of operating conditions on the rejection of cobalt and lead ions in aqueous solutions by a nanofiltration polyamide membrane, J. Membr. Sci., 325 (2008) 150.
[40] C. Gherasim, J. Cuhorka, P. Mikulášek, Analysis of lead (II) retention from single salt and binary aqueous solutions by a polyamide nanofiltration membrane: experimental results and modelling, J. Membr. Sci., 436 (2013) 132.
[41] G. Zeng, Y. He, Y. Zhan, L. Zhang, Y. Pan, C. Zhang, Z. Yu, Novel polyvinylidene fluoride nanofiltration membrane blended with functionalized halloysite nanotubes for dye and heavy metal ions removal, J. Hazard. Mater., 317 (2016) 60.

[42] S.S. Hosseini, A. Nazif, M.A.A. Shahmirzadi, I. Ortiz, Fabrication, tuning and optimization of poly (acrilonitryle) nanofiltration membranes for effective nickel and chromium removal from electroplating wastewater, Sep. Purif. Technol., 187 (2017) 46.
[43] J. Gao, S. Sun, W. Zhu, T. Chung, Chelating polymer modified P84 nanofiltration (NF) hollow fiber membranes for high efficient heavy metal removal, Water Res., 63 (2014) 252.
[44] M.A. Barakat, New trends in removing heavy metals from industrial wastewater, Arab. J. Chem., 4 (2011) 361.